

Degradation modes of crosslinked coatings exposed to photolytic environment

Tinh Nguyen, Xiaohong Gu, Mark Vanlandingham,
Eric Byrd, Rose Ryntz, Jonathan W. Martin

© American Coatings Association & Oil and Colour Chemists' Association 2012

Abstract The objective of this study is to assess the degradation modes of crosslinked coatings exposed to photolytic environments. Three model crosslinked coatings were exposed in various ultraviolet environments. Atomic force microscopy and Fourier transform infrared spectroscopy were used in following nanoscale physical and chemical degradation during exposures. Results indicated that photodegradation of crosslinked coatings is a spatially localized (inhomogeneous) process in which nanometer-sized pits are initially formed; these pits deepen and enlarge with exposure. A conceptual model is proposed to explain the inhomogeneous degradation mode. The model proposes that nanosize “hydrophilic” domains are dispersed randomly with the highly crosslinked units. These hydrophilic domains, which are energetically preferred, comprise polar, unreacted and partially polymerized molecules, chromophores, and other additives. Photodegradation initiates at degradation-susceptible hydrophilic domains spreading to surrounding areas contiguous with the initiation site.

Keywords AFM, Coatings, Crosslinked polymers, Degradation, Heterogeneous, Mode, Photodegradation, UV

Introduction

Polymeric coatings are used extensively in exterior applications, both for aesthetic and protective purposes. However, polymeric materials degrade when exposed outdoors.¹ Among the weathering factors, ultraviolet (UV) radiation inflicts severe damage to polymeric materials through a complex photochemical process. Other weathering factors, such as moisture, temperature, and pollutants, act synergistically with UV radiation amplifying UV-induced degradation. For a typical polymeric coating to undergo photodegradation during exposure to terrestrial sunlight, two critical conditions must be satisfied: solar radiation must be absorbed by the coating film and the absorbed radiation must have sufficient energy to break the bonds of the polymers. Neither requirement is met for pure polymers because their bonds do not absorb any appreciable amount of radiation >295 nm.² The fact that polymeric materials undergo photodegradation during exposure to solar radiation (>295 nm) indicates that chromophores are present.³ Chromophores, such as residual initiators, antioxidants, impurities, etc., are capable of absorbing light at low wavelength and initiating oxidative reactions of the polymer chains. Photodegradation of polymers exposed to sunlight is, therefore, a photo-oxidation process, which is responsible for the chain scission, mass loss, as well as the formation of peroxide and carbonyl groups. Some photo-oxidative products absorb radiation in long wavelengths and accelerate the degradation of the polymer chains. These chromophores are not necessarily uniformly dispersed throughout the polymer

This paper was presented by Tinh Nguyen, the 2011 ACA Mattiello Memorial Lecturer, as part of the Mattiello Lecture presentation at the CoatingsTech Conference, sponsored by ACA, March 14-16, 2011, in Rosemont, IL.

T. Nguyen (✉), X. Gu, M. Vanlandingham,
E. Byrd, J. W. Martin
National Institute of Standards and Technology,
Gaithersburg, MD 20899, USA
e-mail: tinh.nguyen@nist.gov

Present Address:
M. Vanlandingham
Army Research Laboratory, Aberdeen, MD, USA

R. Ryntz
IAG, Southfield, MI, USA

film, leading to the initiation of degradation at highly localized, nanoscale dimension sites.

The development and advances of scanning probe microscopy, particularly the tapping mode atomic force microscopy (AFM), has made it possible to investigate both chemical and physical degradation at nanoscale dimensions. Tapping mode AFM exerts a very small force and little contact on the sample, and its phase imaging capability can provide contrast of domains that have different properties.^{4–6} Degradation mode is defined here as the physical manifestation of damage to a coating. Information on the degradation mode is essential for better understanding the degradation mechanism and for more precisely predicting the service life of polymeric coatings exposed to the environment. Possible degradation modes include uniform reduction of film thickness and localized pitting of a film surface, i.e., inhomogeneous degradation.

The objective of this study is to assess the degradation mode of crosslinked polymeric coatings exposed to UV environments. To meet this objective, the surface morphological changes at nanoscale spatial resolution and chemical degradation of three model crosslinked coatings exposed to UV radiation are presented to demonstrate the degradation mode. Surface morphological change of a commercial coating system was also studied for comparison. Based on the experimental results, a conceptual model is proposed to explain the degradation mode.

Experimental procedures*

Materials and sample preparation

Three model, unpigmented crosslinked coatings were selected: an amine-cured epoxy, an acrylic urethane, and an acrylic melamine. None of the coatings contained UV stabilizers or additives. The amine-cured epoxy was a stoichiometric mixture of a pure diglycidyl ether of bisphenol A (DGEBA) with an epoxy equivalent of 172 (gram equivalent is defined as the grams of resin containing 1 g equivalent of epoxide) and 1,3-bis(aminomethyl)-cyclohexane (1,3 BAC). Hereafter, the 1,3 BAC–DGEBA system is designated as the amine-cured epoxy. The acrylic urethane was a 65:35 mixture by mass fraction of an acrylic polyol and a conventional biuret hexamethylene diisocyanate. The acrylic polyol resin contained 68% butyl methacrylate, 30% hydroxy ethylacrylate, and 2% acrylic acid. The acrylic melamine coating was a 70:30 mixture by mass of the same acrylic polyol described above and a melamine crosslinking agent. The latter was a mixture

of 69.0% partially methylated melamine resin and 31.0% isobutanol solvent.

For the epoxy coating, the preparation of specimens for investigation of surface morphological and chemical degradation was different. For surface morphological studies, specimens were made by stoichiometrically mixing the resin and amine curing agent thoroughly using a mechanical stirrer. After degassing, the mixture was applied to a urethane-coated aluminum substrate by drawdown in a CO₂-free glove box. Epoxy-coated specimens were cured at room temperature for 48 h, followed by post-curing at 130°C for 2 h. All specimens were well cured, as evidenced by no further Fourier transform infrared spectroscopy (FTIR) intensity decrease of the epoxide band at 915 cm⁻¹. The glass transition temperature, T_g , of the cured epoxy coating was 123 ± 2°C as measured by dynamic mechanical analysis (DMA). The thickness of the epoxy coating layer was 152.0 ± 4.2 μm (the number after the ± sign indicates one standard deviation). In addition, a cryo-fractured 3-mm thick section of the same epoxy film, obtained from a polypropylene mold, was used for characterizing the epoxy's bulk microstructure. The cryo-fractured surfaces were prepared by notching a 12 mm × 12 mm × 3 mm specimen with a band saw, immersing the notched specimen in liquid nitrogen for 1 h, and fracturing it with a screwdriver. Chemical degradation of the epoxy was studied on 8 ± 0.7 μm thick films spin cast on 25 mm diameter CaF₂ plates.

Acrylic urethane and acrylic melamine specimens were prepared by spin casting on 100 mm diameter CaF₂ plates. Accordingly, acrylic polyol, isocyanate, and melamine crosslinking agents in appropriate solvents were mixed at the required ratio, degassed, flooded onto the substrates, and spun at 200 rad/s (2000 rpm) for 30 s. Coated specimens were cured at 130°C for 20 min. The average thickness of acrylic urethane film was 10.2 ± 1.2 μm and that for the acrylic melamine was 8.5 ± 1 μm. Thicknesses of spin-coated specimens (including the spin-coated epoxies) were measured on their cross sections using a scanning electron microscope (SEM). T_g values of the cured acrylic urethane and acrylic melamine coatings were 56 ± 1 and 48 ± 2°C (by DMA), respectively. A specimen used for bulk microstructure measurement of acrylic urethane was prepared following the same procedures described above for amine-cured epoxy bulk microstructure. Chemical structures of three crosslink coatings are illustrated in Fig. 1.

For comparison purposes, morphological changes of a commercial coating system applied to a thermoplastic olefin (TPO) bumper exposed to UV radiation were also studied. This coating system consisted of a clear topcoat, a basecoat, and a primer. The clearcoat was a polyester acrylic binder with added UV light stabilizer, hindered amine light stabilizer, and rheology control modifiers. The basecoat was a polyester urethane system with added rheology control modifiers pigmentation to attain the selected color. The primer was a polyester urethane with added chlorinated polyolefin

* Certain commercial products or equipment are described in this paper in order to specify adequately the experimental procedure. In no case does such identification imply recommendation or endorsement by the National Institute of Standards and Technology, nor does it imply that it is necessarily the best available for the purpose.

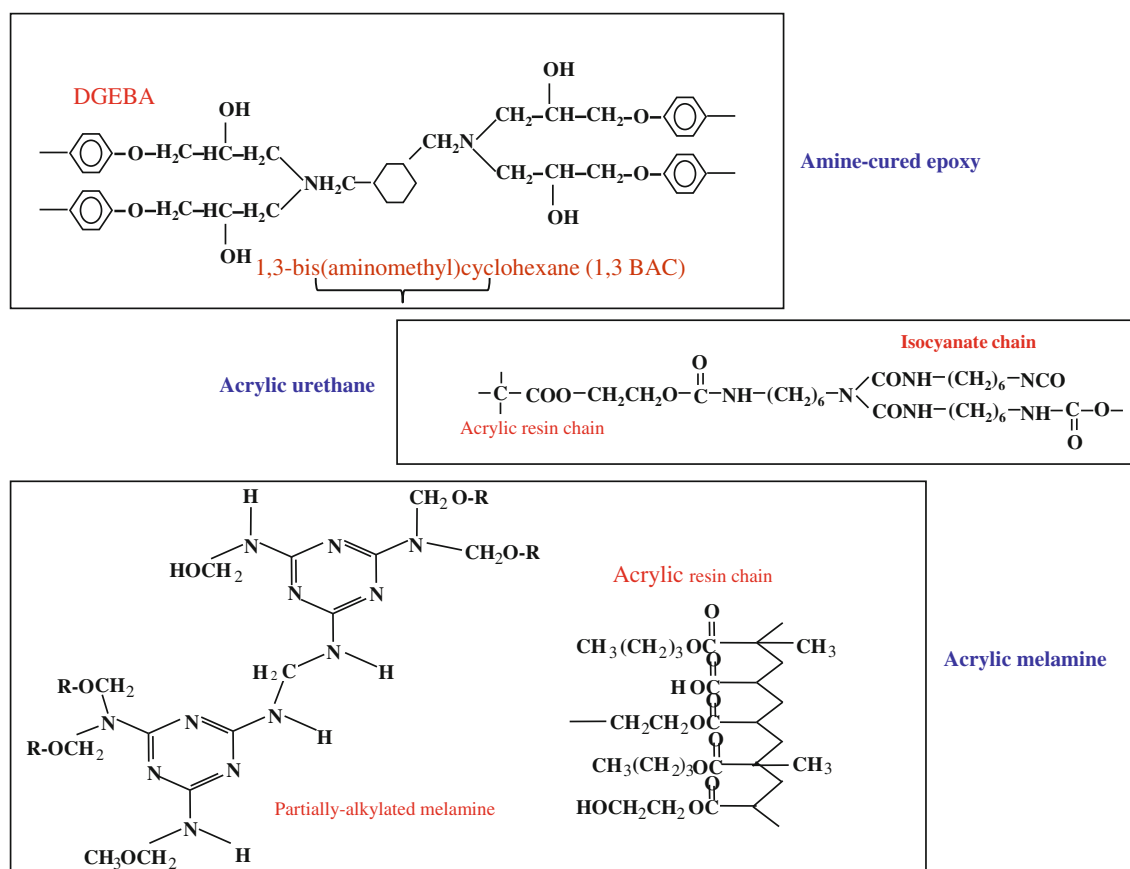


Fig. 1: Chemical structures of the acrylic melamine, acrylic urethane, and 1,3 BAC amine-cured epoxy coatings used in this study

to attain adhesion to the low surface-free energy plastic substrate. Hereafter, this system is termed the acrylic-urethane coating/TPO system.

Exposures and apparatus

Specimens were exposed to different UV conditions. The epoxy coating was exposed outdoors in Gaithersburg, Maryland, using an environmental chamber described previously.⁷ One particular feature of this chamber is that its four sides were enclosed with a vortex material that allowed water vapor, but prevented dust from entering the chamber. This design greatly reduced the deposition and embedment of dust particles into the surface of the coated samples, which could complicate AFM measurements and the interpretation of the results. The acrylic urethane and acrylic melamine coatings were exposed to an artificial UV environment having a relative humidity (RH) of 70% and a temperature of 50°C. A complete description of this UV chamber is given in reference (8). Briefly, specimens were placed in an exposure cell that was equipped with a thermocouple and a RH sensor. The cell consisted of a 12-window aluminum disk, a quartz

plate, and a 100-mm diameter CaF₂ plate that had a film of the coating on it. The cell contained an inlet and an outlet that allowed air having a preselected temperature and RH to continuously enter and exit the exposure cell. The temperature within each exposure cell was controlled to within ±1°C. The RH flowing to the sample was supplied by a humidity generator. The RH could be independently controlled and maintained to within ±3% its preset value. The UV light source consisted of a 1000 W xenon arc lamp emitting radiation having wavelengths from 275 to 800 nm. The UV source was equipped with an optical system that removed the major portion of the infrared and visible radiation from the flux. The intensity of the flux was maintained over the duration of the experiment via a photofeedback controller. For acrylic urethane coating, a 300 nm cut-on filter was inserted between the specimen and the light source to remove all radiation below approximately 300 nm. On the other hand, specimens of acrylic melamine were exposed to the full UV spectrum of the xenon arc source (i.e., from 275 to 800 nm). The UV intensity increased linearly with exposure time. The total doses of the 300 nm cut-on filter and by the full UV lamps recorded at 100 days were 2512 kJ/m² and 2950 kJ/m², respectively.

Commercial acrylic-urethane coating/TPO specimens were exposed in a commercial weatherometer equipped with borosilicate glass inner and outer filters. The exposure cycle was run according to SAE J1960, which has the following characteristics:

Parameter	Dark cycle	Light cycle
Irradiance	NA	0.55 W/m ² @ 340 nm
Black panel temperature	38°C	70°C
Conditioning water	40°C	45°C
Relative humidity	95 ± 5%	50 ± 5%

Degradation measurements

Surface morphological changes (physical degradation) at nanoscale spatial resolution were studied by AFM while chemical degradation was characterized using FTIR in the transmission mode (T-FTIR). AFM measurements were made using a Dimension 3100 Scanning Probe Microscope (Bruker) operated in tapping mode and commercial Si microcantilever probes. Tapping mode operation was used because it causes minimal damage to the sample while maintaining high spatial resolution. Changes in phase angle of the oscillating probe during scanning in the tapping mode (i.e., phase image) often provide significantly more contrast than those obtained from a topographic image. This is helpful for studies of coatings microstructure where differences between regions in a cured film are subtle but are important in degradation investigation. Both topographic (height) and phase images were obtained simultaneously using a resonance frequency of approximately 300 kHz for the probe oscillation and a free-oscillation amplitude of 62 ± 2 nm. The set-point ratio (the ratio of set point amplitude to the free amplitude) ranged from 0.60 to 0.80. For acrylic urethane and acrylic melamine coatings, a special holder was used to follow surface morphological changes at the same location. A detailed description of the holder and experimental protocol of this measurement are provided in reference (9). Transmission FTIR spectra were measured using an automatic sampling device described previously.¹⁰ All T-FTIR spectra

were the average of 128 scans, which were recorded at a resolution of 4 cm^{-1} using a liquid nitrogen-cooled mercury cadmium telluride (MCT) detector, and dry air was used as the purge gas. The peak height method was employed to represent IR intensity, which is expressed in absorbance units, A. Only difference T-FTIR spectra (obtained by directly subtracting the spectrum of the unexposed specimen from the spectrum of the exposed specimen) are presented in this article, because our previous studies^{7,8,10} have clearly demonstrated that difference FTIR spectra provide more detailed information about chemical changes than spectra recorded at each exposure time.

Results and discussion

Amine-cured epoxy

Figures 2a and 2b display AFM images taken from the surface (film/air interface) and the bulk, respectively, of the amine-cured epoxy before exposure. The surface image was obtained on the 150- μm thick film applied to the polyurethane-coated aluminum substrate sample used for the outdoor exposure, and the bulk image was from the cryo-fractured 3 mm thick section of the same epoxy, as presented in the experimental section. The bright and dark areas in the topographic images correspond to the higher and lower topography, respectively, relative to the averaged plane of the imaged region.

Both topographic and phase images of Fig. 2a show that the air/film surface is smooth and contains slightly bright and faintly dark domains. Examination of phase images taken from a variety of amine-cured epoxies reveals that the air surface of this type of epoxy is a generally featureless, textured pattern.^{11–13} The smooth and less-defined microstructure of the air surface has been attributed to the presence of a very thin layer of a lower surface-free energy material. Extensive measurements using AFM as well as other surface analytical techniques have shown that the outer surface of a multicomponent polymer system is generally enriched with a lower surface-free energy

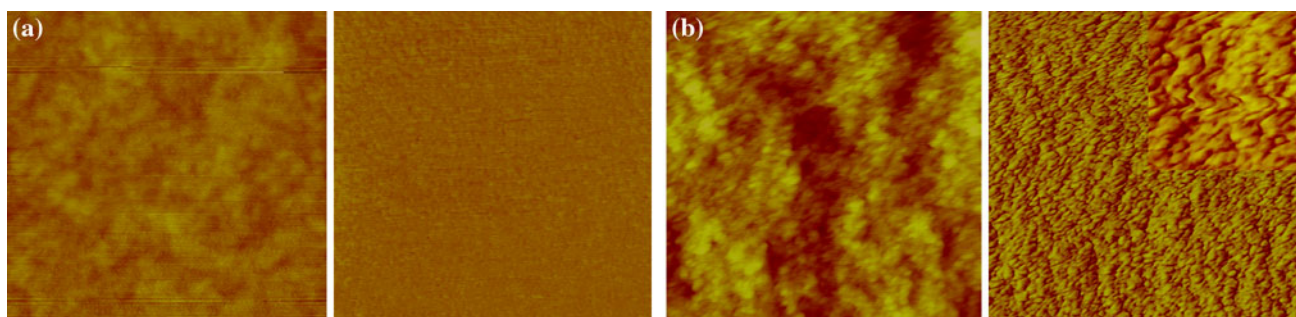


Fig. 2: $1 \mu\text{m} \times 1 \mu\text{m}$ AFM topographic and phase images of the surface (a) and the bulk (b) of a 1,3 BAC amine-cured epoxy. For each image pair, the topographic image is on the left and phase image is on the right. The inset is the $250 \text{ nm} \times 250 \text{ nm}$ phase image, revealing small, dark regions are interspersed in the bright regions

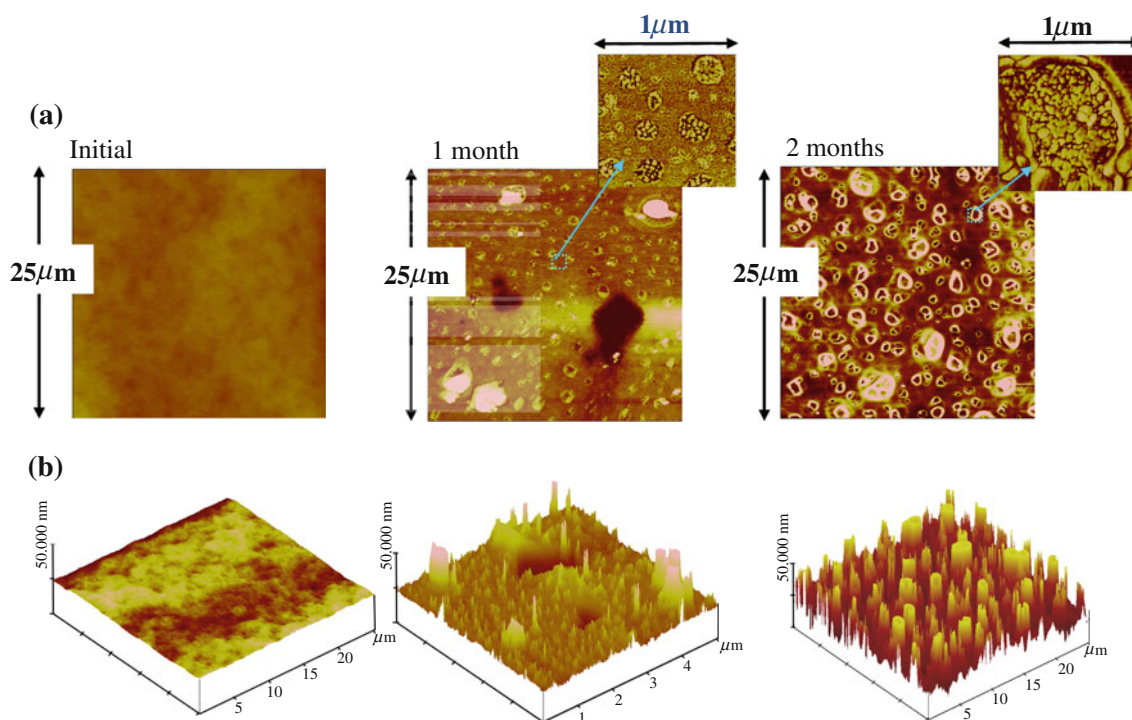


Fig. 3: 25 $\mu\text{m} \times 25 \mu\text{m}$ 2-D (a) and 3-D (b) AFM topographic images of the amine-cured epoxy before and after exposure to the outdoors in Gaithersburg, MD, for 1 and 2 months, started from the middle of July. Insets are high magnifications of the phase images

component to minimize polymer–air interfacial energy.^{14,15} This thin surface layer could mask the underlying microstructure from being detected by an AFM probe.

The phase image of the bulk (Fig. 2b, right) shows that this amine-cured epoxy material has a nodular microstructure, which is due to the heterogeneity in crosslinked polymers, as elaborated later in the inhomogeneous degradation conceptual model. An examination of the higher magnification phase image (Fig. 2b, inset) reveals that interspersed in the bright regions are smaller, darker regions. A similar two-phase structure has also been observed for bis(*para*-aminocyclohexyl) methane-cured epoxy,¹⁶ amine-cured epoxy,^{12,13} and crosslinked polyester.¹⁷ The bright domains in the phase image have been found to be mechanically harder than the surrounding darker regions.^{18,19} Based on this assignment, it is reasonable to conclude that the bulk microstructure of this amine-cured epoxy is heterogeneous, consisting of a minor fraction of softer material (dark) dispersed in a harder matrix (bright). Further, the harder matrix and softer material in an epoxy have been attributed to the highly crosslinked and low-crosslinked regions, respectively.^{16,20,21}

AFM topographic images obtained on the same epoxy before and after exposing for 1 and 2 months outdoors in Gaithersburg, Maryland, are displayed in Fig. 3. The exposure started in the middle of July, and solar dose values measured after 1 and 2 months were 9100 and 20614 kJ/m², respectively. Our previous exten-

sive study has clearly demonstrated that UV radiation is the main weathering element that causes severe degradation of amine-cured epoxies, with temperature and RH playing a minor role.⁷ As seen in Fig. 3, the degradation, i.e., the photodegradation, of this amine-cured epoxy is not a homogeneous process. After 1 month, regular-spaced degradation features appeared interspersed with two large pits, and the pit diameters ranged from a few nanometers to hundreds of nanometers, but the depths of these pits were only a few nanometers. After 2 months of exposure, the regular-spaced degradation features increased in number and became more pronounced, and the pits became deeper and larger. Interspersed with the pits were protuberances or domes, which are attributed to degradation products.⁹ The regular-spaced features only appeared late in the exposure and were observed only in the case of specimens exposed outdoors. Water condensation, heterogeneous microstructure, and hydrolysis of the oxidized products all may play a role in the formation of these features. High-resolution 2-D phase images (Fig. 3a, insets) revealed that the degraded regions after 1- and 2-month exposures exhibit a two-phase pattern that resembles the nodular structure observed in the bulk microstructure shown in Fig. 2b and in the interior surface (surface in contact with the substrate during film formation) microstructure reported in references (12) and (13).

Substantial chemical degradation has occurred in this amine-cured epoxy, as demonstrated by the

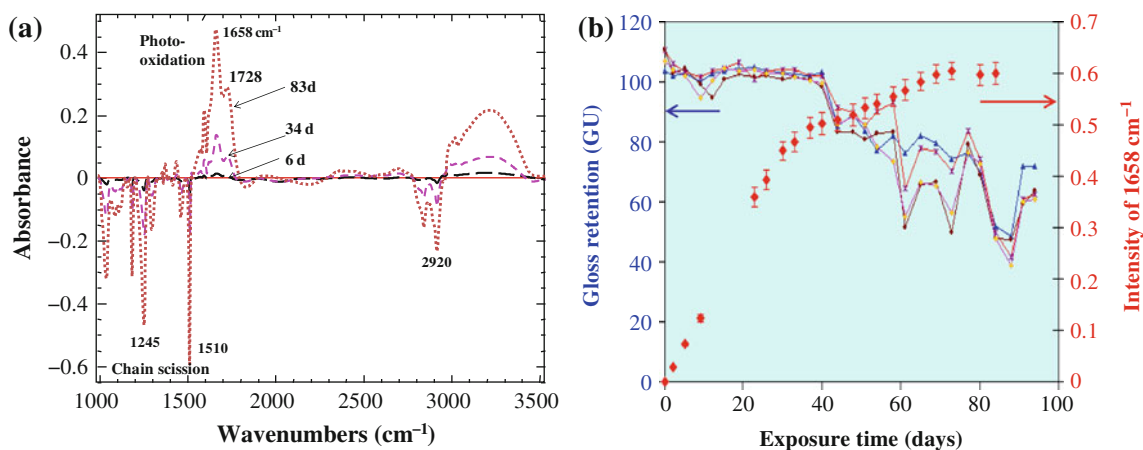


Fig. 4: Chemical degradation and gloss loss of the amine-cured epoxy exposed to the outdoors in Gaithersburg, MD. (a) Difference transmission FTIR spectra at three exposure times, and (b) oxidation increase and gloss loss as a function of exposure times. Data of four individual specimens are shown for the gloss, while data for the oxidation are the average of four specimens (error bars for the intensity/time curve represent one standard deviation)

spectroscopic results shown in Fig. 4. Difference T-FTIR spectra (Fig. 4a) exhibit substantial intensity decreases of numerous bands of the epoxy structure, e.g., at 1245 and 1510 cm^{-1} , due to the aryl-O bonds and the benzene ring, respectively, with increased exposure while at least two peaks appeared, the bands at 1728 cm^{-1} , due to C=O stretching of a ketone, and 1658 cm^{-1} , assigned to amide C=O stretching.^{22,23}

The appearance of these bands is in good agreement with a photo-oxidative mechanism proposed previously for epoxy cured with aliphatic amines.^{23,24} Ketone formation is derived from the secondary hydroxyl groups, while amide is generated from the abstraction of a hydrogen from the methylene groups adjacent to the crosslink. Generated carbonyl species absorb radiation at long UV wavelengths and this absorption leads to photodegradation. UV-visible spectra (not shown) exhibited a progressive absorbance intensity increase in the region above 300 nm, indicating that the degraded epoxy films begin to absorb UV light at longer wavelengths. The extent of degradation of the epoxy is exhibited in Fig. 4b, which displays the oxidation rate and gloss loss with exposure time. The oxidation was almost linear for the first 40 days after which it began to level off. On the other hand, the loss of gloss hardly changed at all from its initial value for the first 40 days but started to decrease thereafter, suggesting that prior to any physical manifestation of damage, significant chemical changes have already occurred. Further, a comparison of AFM results in Fig. 3 and gloss data of Fig. 4 suggests that the nanoscale surface morphological changes that occurred during the first month of exposure had little effect on the gloss loss while subsequent changes to the morphology had a significant impact on gloss. The loss of gloss also implied that the surface degradation was a localized process, as directly observed by AFM. This is because glossiness is a direct function of a surface's

specular reflection. If the degradation is a uniform thickness loss from the surface, there should be no change in the specular reflectivity or gloss of the specimens with exposure.

Acrylic urethane

Figure 5 displays 2-D AFM images of the surface (film/air) and the bulk of the acrylic urethane coating. Similar to those of the epoxy, both topographic and phase images show that the air surface is relatively smooth and homogeneous. On the other hand, except for the slight distortion due to the fracturing process, the phase AFM image of the bulk microstructure exhibits bright and dark patterns similar to those of the bulk and microtomed surface of amine-cured epoxies. This result suggests that the bulk microstructure of an acrylic urethane coating is heterogeneous, consisting of softer regions (dark) dispersed in a harder matrix (bright), similar to that of amine-cured epoxies and polyester, as indicated earlier.

Topographic AFM images of the acrylic urethane coating exposed for different times in the xenon arc UV radiation that had a 300 nm cut-on filter between the specimen and the light source are presented in Fig. 6. These images were taken approximately at the same location near the center of the sample. This figure shows clearly that the degradation is not uniform but, instead, it is highly localized. Two circular pits were visible after 34 days (843 kJ/m^2) and these pits remained the dominant morphological feature at this specimen location for the next 120 days. After 5 months, additional pits have emerged and regularly spaced protuberances have appeared on the entire exposed surface of the film. After 250 days (6200 kJ/m^2) of exposure, many pits have appeared on the coating surface and the pits became rather deep (e.g., Fig. 6b, far left). In addition, acrylic

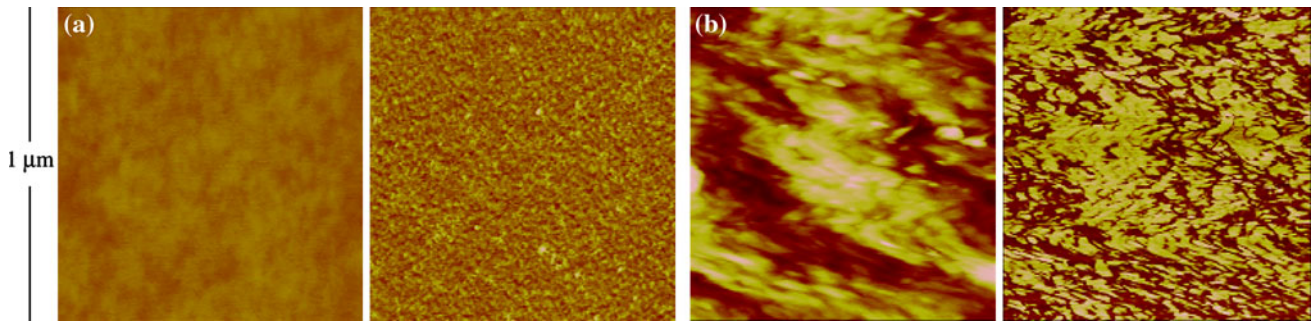


Fig. 5: 1 $\mu\text{m} \times 1 \mu\text{m}$ AFM topographic and phase images of the surface (a) and the bulk (b) of the acrylic urethane coating. In each image pair, the topographic image is on the left and phase image is on the right

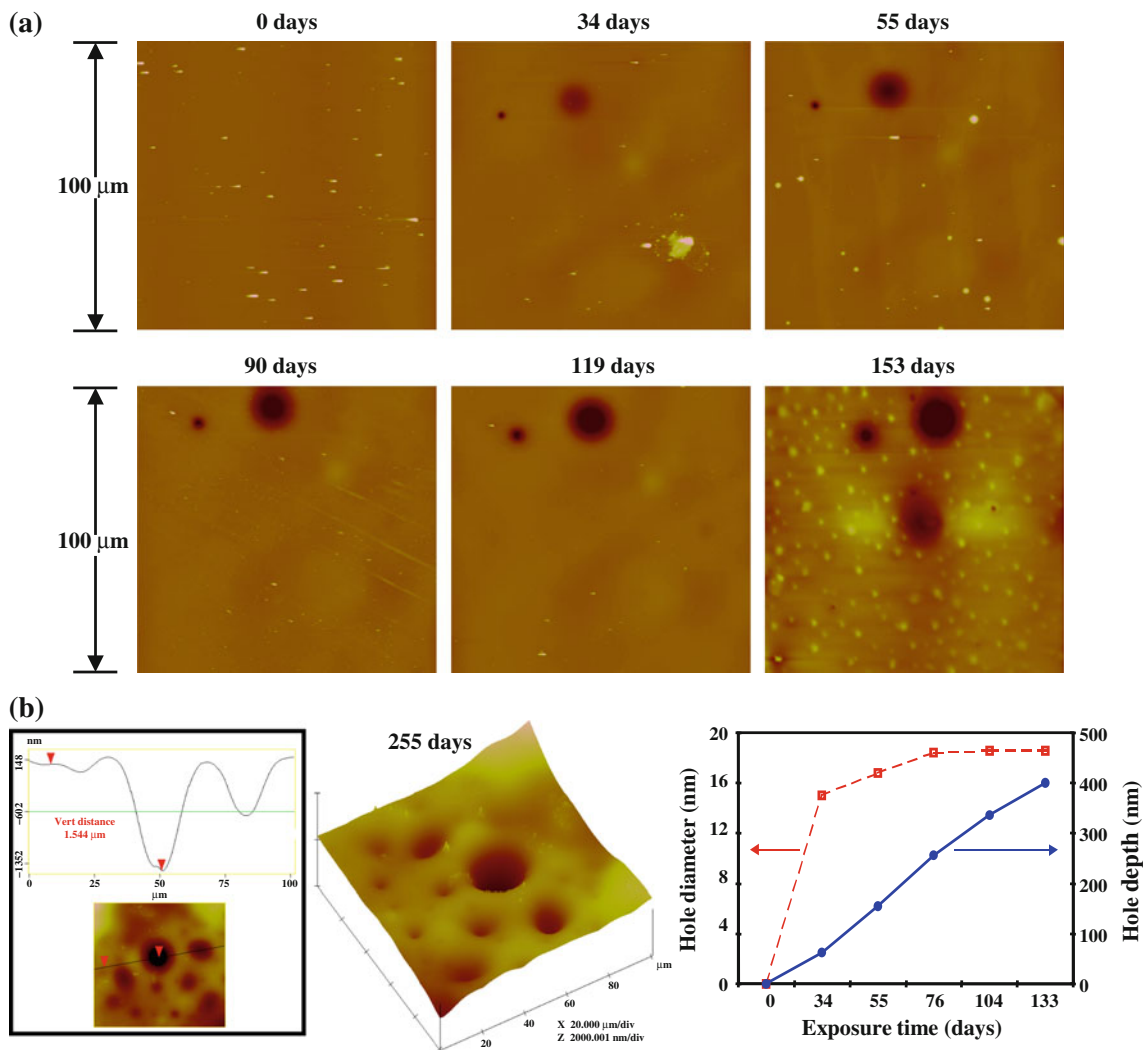


Fig. 6: (a) 100 $\mu\text{m} \times 100 \mu\text{m}$ 2-D topographic AFM images of the acrylic urethane coating exposed to UV radiation at 70 % RH and 50°C for different times; images were taken at approximately the same location. Dark circles are pits and bright spots are protrusions; (b) from left to right, 100 $\mu\text{m} \times 100 \mu\text{m}$ 2-D images with line profile after 255 days' exposure, the corresponding 3-D image, and change of a pit's depth and diameter with exposure time

urethane specimens subjected to monochromatic UV radiation at 294 and 312 nm wavelengths under the same temperature/RH condition also exhibited similar local-

ized degradation, with the formation of numerous pits (not shown). However, the depth and diameter of the pits were smaller than those under polychromatic

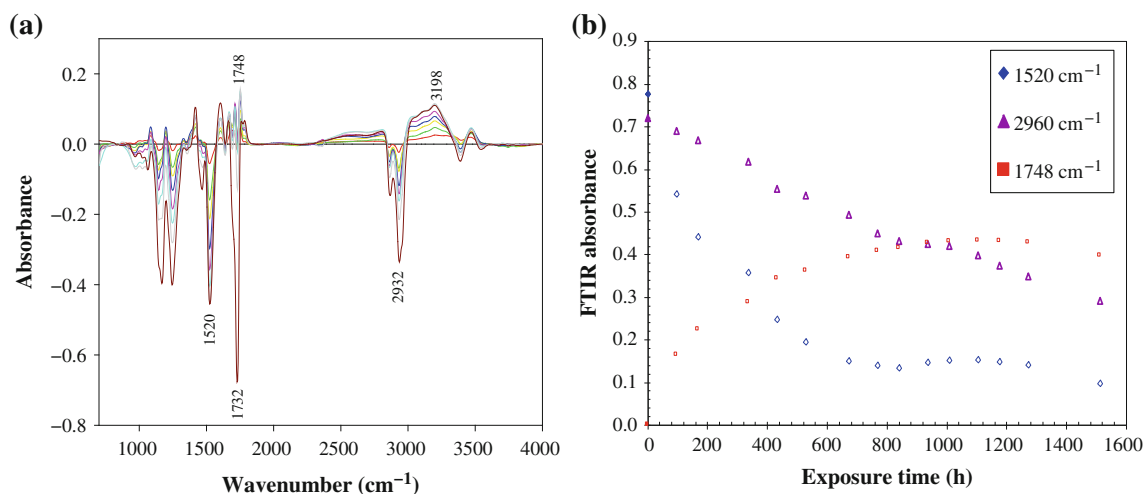


Fig. 7: Chemical degradation of the acrylic urethane coating exposed to 300 nm cut-on filter UV at 50°C and 70% RH: (a) difference transmission FTIR spectra, and (b) FTIR intensity changes with exposure time of several bands, showing substantial degradation has occurred

radiation. From these and other^{9,13,17} results, it can be concluded that the AFM provides a powerful tool for tracking morphological changes, e.g., the enlargement and deepening of locally degraded regions in the coating film at the nanoscale dimension, as a function of time exposed to the UV environments. One example is demonstrated in the graph of Fig. 6b (far right pane). It shows that the pit depth appeared to increase almost linearly with time while the diameter initially enlarged rather quickly then became almost constant at long exposure. It should be cautioned that because only one scan was used for the analysis, no uncertainty ranges can be given for this graph. In addition, these results are presented to demonstrate the quantitative capability of AFM for study of coatings degradation at the nanoscale spatial resolution and should not be generalized for all pits.

The chemical degradation of this acrylic urethane coating is illustrated in Fig. 7, which shows difference T-FTIR spectra and band intensity changes with exposure time. Bands in various regions have increased and decreased with exposure to the humid, warm UV environment. Of particular interest is the occurrence of the 1748 cm^{-1} band, due to C=O of acetylurethane ($\text{O}=\text{C}-\text{NH}-\text{O}-\text{C}=\text{O}$),²⁵ and the intensity loss of the 1520 cm^{-1} band, due to amide II (NH bending and CH stretching). The formation and loss of these bands represent the oxidation and chain scission, respectively, of the coating. Figure 7b also shows a decrease in intensity with exposure time of the 2960 cm^{-1} band, due to CH_3 , indicating the loss of this hydrocarbon group. The FTIR spectral changes observed in Fig. 7 are in good agreement with a photo-oxidation mechanism proposed for acrylic urethane coating exposed to UV radiation in the absence or presence of moisture.²⁵ In the presence of oxygen and UV light, the urethane groups are oxidized to form acetylurethane, which is easily

hydrolyzed by water to form acids and urethane. The acrylic resin portion also undergoes degradation to form a number of oxidized products, such as acids and alcohol.

Figure 8 displays AFM topographic images of the commercial acrylic-urethane coating/TPO system before and after 1500 kJ/m^2 exposure in a xenon arc weatherometer whose characteristics are given in the experimental section. In Fig. 8, 3-D images are on the left and 2-D images and line profiles are on the right. It should be mentioned that, because AFM only detects features that are of a few nanometers from the surface, the results in Fig. 8 were from the surface of the topcoat, i.e., of the clear polyester acrylic film.

Before exposure, the coating surface was very smooth having a root mean square roughness (RMS) of less than 1 nm, with no evidence of holes or pits on the surface (Fig. 8, top right). After UV exposure, many pits having diameters in the 150–250 nm range and depths of 5–10 nm (Fig. 8, line profile, lower right) have occurred over the entire surface. This result provided supporting evidence that photodegradation of the topcoat of a commercial acrylic-urethane/TPO coating system is also an inhomogeneous process with the characteristic formation of nanometer size pits. These very small pits should not have an effect on glossiness of the topcoat.

Acrylic melamine

AFM images of air/film surface and interior surface of this acrylic melamine coating have been presented in reference (26). They showed that the acrylic melamine coating also has a two-phase microstructure, similar to that of the amine-cured epoxy and acrylic urethane coatings. 2-D AFM images of the acrylic melamine

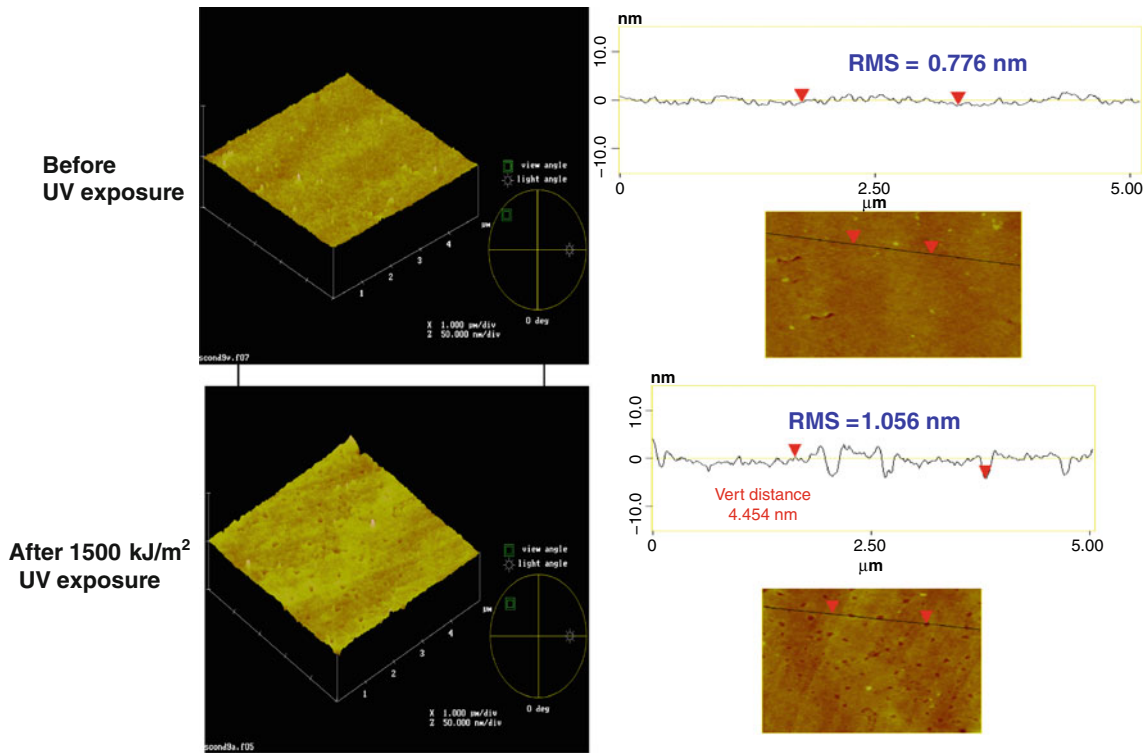


Fig. 8: 5 μm × 5 μm 3-D AFM topographic images (left) and line profiles (right) of the commercial acrylic-urethane/TPO coating system before and after exposure to 1500 kJ/m² in a xenon arc weatherometer, showing nanosize pits formed on the entire surface after the UV irradiation

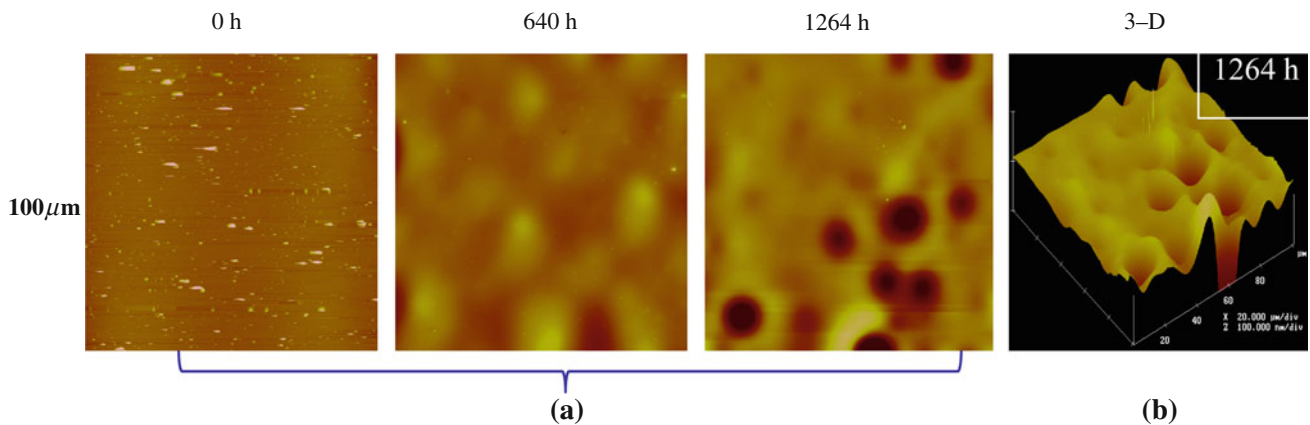


Fig. 9: (a) 100 μm × 100 μm 2-D AFM topographic images of the acrylic melamine coating taken at different exposure times, and (b) 3-D topographic image of the same specimen after 1264 h exposure, showing inhomogeneous degradation with large, deep pits

coating exposed to the full UV spectrum of the xenon arc source for different exposure times are displayed in Fig. 9a. Figure 9b is the 3-D AFM image of the 1264 h (~1540 kJ/m²) exposure specimen. The temperature/RH condition in the exposure chamber for this coating was the same as that for the acrylic urethane, i.e., 50°C and 70% RH.

These images are part of our results reported in references (9) and (27); they are presented here for

completeness. Figure 9 clearly shows that photodegradation of an acrylic melamine coating in a humid UV environment is a localized, inhomogeneous process, similar to that observed for amine-cured epoxy and acrylic urethane coatings.

In Fig. 10, chemical degradation of the acrylic melamine coating exposed to full UV, 50°C and 70% RH is displayed. Difference T-FTIR spectra (Fig. 10a) show intensity decreases and increases in various

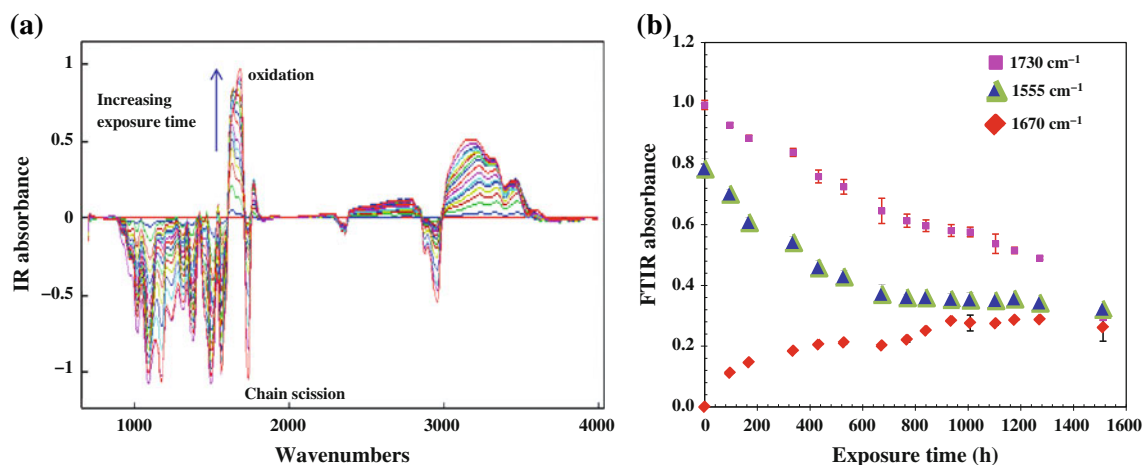


Fig. 10: Chemical degradation of the acrylic melamine coating exposed to full UV at 50°C and 70% RH: (a) difference transmission FTIR spectra, and (b) FTIR intensity changes with exposure time of several bands, showing substantial degradation has occurred

spectral regions with exposure to the humid, warm UV environment. Under UV light, the degradation of acrylic melamine initiates at the CH_2 groups located at the α position of the nitrogen atom in the melamine chain,²⁵ leading to the formation of various oxidized products including amide, alcohol and acids.^{10,25,28} Of particular interest are the bands at 1555 cm^{-1} , attributed to melamine triazine, and at 1670 cm^{-1} , due to amide $\text{C}=\text{O}$. The intensity decrease and increase of these bands represent chain scission and oxidation, respectively. Intensity changes of several bands with UV exposure time are displayed in Fig. 10b. The chain scission was rapid in the first 650 h but became nearly constant thereafter. The oxidation process was also fast at first but slowed down after 500 h.

Figure 10 also shows an intensity decrease of the band at 1730 cm^{-1} , due to $\text{C}=\text{O}$ of the acrylic polyol, indicating that this component also underwent degradation under this UV condition. The photodegradation rate of acrylic melamine in humid UV environment has been found to be much greater than that in dry UV conditions.^{10,28} Further, both oxidation and chain scission processes are more sensitive to humidity than the loss of the acrylic $\text{C}=\text{O}$ groups.²⁷

Conceptual model for the inhomogeneous degradation

The AFM results presented above have indicated that the degradation of a crosslinked coating exposed to UV environments is an inhomogeneous, localized process in which degradation mainly initiates at isolated nano or micro-domains, resulting in the formation of nanoscale pits. Over time, these pits deepen and their diameters enlarge. Inhomogeneous degradation mode is characterized by the formation of a heterogeneous microstructure

nonuniformly dispersed across an AFM image from the three crosslinked coatings used in this study and from previously published AFM results for other crosslinked polymers.^{11,16,17} The microstructure of a variety of crosslinked coatings, including epoxy, phenolic, phthalate polyester, polyurethane, and alkyd have been reviewed in detail.^{26,29} The conclusion from this review is that most, if not all, crosslinked coatings are heterogeneous materials containing a small fraction of low molecular mass, low-crosslinked domains (sol fractions) interdispersed with highly crosslinked units (gel fractions). The formation of heterogeneous structure in crosslinked polymers has been attributed to the incomplete polymerization in the final stage of curing.^{30,31} That is, unreacted and partially polymerized molecules are unable to merge into the highly crosslinked units and left at the periphery of these units during the termination stage. We have designated the low molecular mass, low-crosslinked domains as the “hydrophilic domains” because they behave like a hydrophilic, ion-exchanged membrane²⁶; that is, they take up a large amount of water (45–75%), swell substantially, and have a high ion diffusion coefficient.^{32,33} For commercial coatings, the hydrophilic domains may also contain residual initiators, additives, chromophores, and catalysts because these are short chain, polar molecules, which are readily attracted to the hydrophilic domains via hydrogen bonding. During curing and service, some of the smaller hydrophilic domains diffuse and merge with the larger ones, forming larger but fewer hydrophilic domains in a coating film.

When subject to an aggressive environment, such as UV light, degradation initiates in the hydrophilic domains, leading to the formation of pits. These pits deepen and enlarge from these domains to the surroundings with exposure time, resulting in inhomogeneous, localized degradation. Some smaller pits in close proximity coalesce into larger ones, such that, at long exposure, coalesced and deep pits dominate the

surface topography.³⁴ Although AFM images of coating surface morphologies are presented, it is expected that the bulk coating undergoes similar inhomogeneous degradation. A similar inhomogeneous degradation process has been reported for photo-oxidative and thermal degradation of thermoplastic semicrystalline polymers.^{35,36}

Postulation that crosslinked polymeric coatings consist of hydrophilic domains dispersed in crosslinked units has been experimentally demonstrated by electron microscopy, small angle neutron scattering (SANS), and other techniques. For example, secondary electron microscopy (SEM) images obtained during water sorption in a number of crosslinked polymers clearly showed that water does not diffuse uniformly in these materials, but, instead, preferentially diffuses along the boundaries between crosslinked units.²⁹ Similarly, SANS and transmission electron microscopy (TEM) studies clearly revealed that the hydrophilic carboxylic acid compounds in carboxylated styrene-butadiene latex films mostly concentrate at the particle-particle interfaces and that water transport in these latex films is mainly along these hydrophilic interfaces, and not through the crosslinked particles.³⁷ The first direct chemical evidence of inhomogeneity in a crosslinked polymer film was provided by a high-resolution near infrared multispectral imaging technique.³⁸ This study showed that the reaction rates within an epoxy sample are inhomogeneous and the difference in the degree of cure at different locations can be as high as 37%. Results of other studies also support the presence of hydrophilic domains or hydrophilic materials in crosslinked coatings. For example, microhardness and DC resistance measurements suggested that crosslinked coatings consist of “conducting polymer phase” dispersed in the polymer matrix, and that corrosion occurs directly underneath the conducting phase.^{39,40} A study using array microelectrodes has reported that phenolic, polyurethane, and alkyd coatings contain low DC resistance regions where conductive pathways develop and enlarge during exposure to electrolyte that allow ion transport through the coating films to the substrate.⁴¹ Water extraction of cured alkyd and epoxy ester coatings also showed that these materials lose about 4–5% of their initial mass,⁴² indicating that these coatings contain low molecular mass, water-soluble materials.

A number of compelling reasons exist for explaining why degradation preferentially initiates in the hydrophilic domains rather than in the crosslinked units. First, under the same exposure conditions, the rate of both photodegradation and hydrolysis reactions is generally greater for small, low molecular mass molecules than for their high molecular mass counterparts. For example, the sol fraction (i.e., the low molecular mass fraction) of both the polysulfone and phenoxy has been shown to carry the bulk of photo-oxidation of these resins in air.⁴³ Similarly, several studies have demonstrated that the rate of hydrolysis is greater for smaller or partially crosslinked molecules than their

higher molecular mass or fully crosslinked counterparts.^{44–46} Second, for photo-oxidation to occur, chromophores and oxygen must be present, and high densities of these species are more likely to be found in the soft, low-crosslinked, hydrophilic domains than in the rigid, highly crosslinked units. Similarly, for hydrolysis to occur and be sustained, both the amount of water and its rate of transport into the reaction sites must be substantial. Other factors, such as mobility of free radicals and ease of degradation products removal, are essential for sustaining the degradation reactions. These requirements are more easily met or facilitated in the soft, low molecular mass, hydrophilic domains than in the rigid, highly crosslinked units. It is noted that hydrolysis is mentioned sometimes in this paper, because for some coatings such as acrylic melamine,^{27,28} both hydrolytic and photodegradation occur simultaneously when they are exposed to a humid UV environment, such as the condition used in this study, or to the outdoors.

Figure 11 schematically presents a proposed heterogeneous microstructure model, which shows hydrophilic domains interdispersed with crosslinked units. Depending on the degree of cure and chemical composition, some of these hydrophilic domains may be interconnected. Because the hydrophilic domains contain a variety of polar groups, such as OH, NH, C=O, it is expected that these groups interact with each other strongly through hydrogen bondings (H-bondings). Further, because polymer chains of the crosslinked units also contain electronegative atoms such as O and N, they can form hydrogen bonds (red-dashed lines in Fig. 11) with the replaceable H atoms in the hydrophilic domains. This model is similar to our previously proposed one²⁶ to explain the localized hydrolytic degradation of an acrylic melamine, except that, in addition to the low molecular mass, partially polymerized molecules, the present model also includes chromophores, residual initiators, and impurities that are responsible for absorbing UV light and initiating the photochemical reactions. It is also similar to Gierke’s model⁴⁷ that describes the cluster of nanoaqueous subphase (i.e., hydrophilic domains) in Nafion membrane. Nafion consists of a poly(tetrafluoroethylene) backbone and acid side chains; the latter forms hydrophilic domains having a size of ~2 nm in dry state. In the presence of water, these nanohydrophilic domains swell, link together, and become a proton conductor.

The driving force for the formation of this type of heterogeneous structure in polymer coatings is that the polar molecules in a coating mixture prefer to associate with each other (likes attract likes) instead of randomly dispersing in the mixture; that is, the polar, low molecular mass, unreacted and partially polymerized molecules, residual initiators, impurities, and chromophores prefer to interact (via hydrogen bonding) with each other to form clusters (i.e., hydrophilic domains) rather than to interact with the nonpolar molecules in the matrix. The attraction between polar

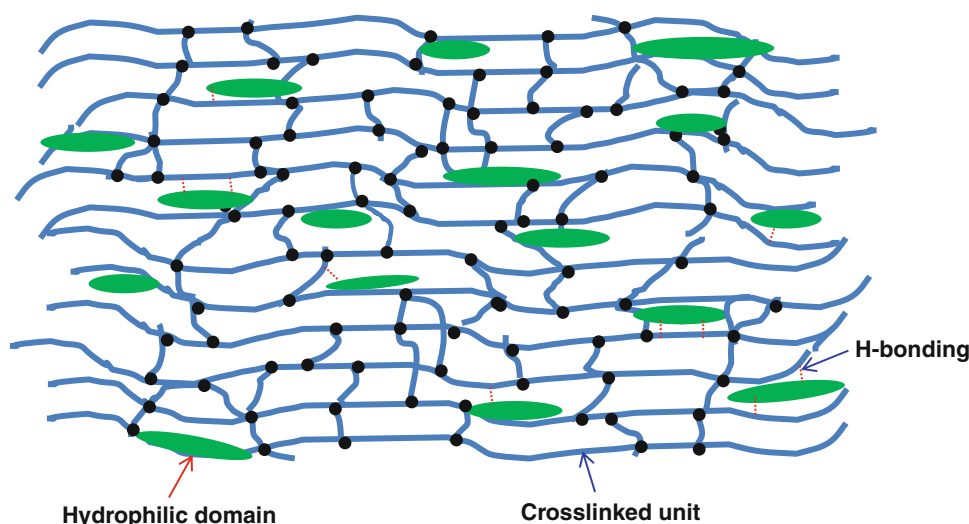


Fig. 11: Conceptual model of the hydrophilic domains in a crosslinked coating (Color figure online)

molecules to form the hydrophilic domains in a polymer coating is consistent with the molecular force interaction principle,⁴⁸ which is applicable to interactions between molecules, particles, surfaces, and multi-component mixtures. According to this principle, the associated state of like molecules is energetically preferred to the dispersed state. For systems that contain polar and nonpolar molecules, the difference in binding energy between the associated state and the dispersed state is large enough (highly negative) to overcome the disordering energy. Such large differences in binding energy will lead to phase separation in a mixture. Further, because the binding energy difference (between associated and dispersed states) is proportional to the number of molecules, large particles or macromolecules are more likely to phase separate than smaller particles or smaller molecules.⁴⁸

The proposed chemically heterogeneous structure shown in Fig. 11 can adequately explain the inhomogeneous photodegradation observed in this study. Specifically, the hydrophilic domains are more reactive and more susceptible to the UV environment than are the crosslinked units. The highly reactive degradation products generated during exposure, such as free radicals, carbonyls, peroxides, acids, etc., are mostly confined in the hydrophilic domains and their vicinities and can accelerate the photoreactions. The result is a deepening and enlargement of the initially degraded regions. It should be noted that, although the degradation initially occurs in the hydrophilic regions in a crosslinked coating, it will spread to other regions of the film as time of exposure increases, leading to loss of film thickness, as observed previously.²²

The understanding of degradation mode proposed in this study, which is based on AFM nanoscale physical degradation, coating microstructure, and extensive literature on the structure of crosslinked polymers is

not complete at this time. It is hoped that future research on better identification and characterization of chemical properties at nanoscale spatial resolution of the heterogeneous domains and degraded regions of polymer coatings will provide a more definitive answer to the degradation mode of coatings exposed to aggressive environments. Nanoscale spatial resolution chemical techniques, such as chemical force microscopy and imaging, AFM Raman spectroscopy, and single molecule spectroscopy, will potentially impart the information needed for a better understanding of the degradation processes and reactions in the hydrophilic domains. Nevertheless, information on the degradation mode provided by this study should help to develop better conceptual and mathematical models for predicting the service life of crosslinked polymeric coatings exposed to UV environments. For example, because the photodegradation of crosslinked coatings is not a uniform thickness loss process, using residual thickness for predicting the service life of these materials exposed to UV may not be a sound approach. Further, information on the degradation mode and the nature of the regions where the photodegradation reactions initiate should help to design more environmentally stable coatings, e.g., minimizing the hydrophilic domains fraction in the film by controlling the reaction conditions such that most of the unreacted and partially polymerized molecules would go to completion and/or by decreasing the concentration of chromophores in the products.

Conclusions

The degradation mode of three crosslinked coatings subjected to various UV environments has been investigated. AFM was used to measure nanoscale

physical degradation and FTIR in the transmission mode was employed to follow chemical degradation. High spatial resolution AFM images clearly showed that crosslinked coatings have a heterogeneous microstructure. The degradation of these materials under UV radiation is not a uniform loss of thickness but is a highly localized, inhomogeneous process, with pits forming and growing at some locations and not at others. Once formed, the pits deepen and enlarge with increased exposure. A conceptual chemically heterogeneous structure model is proposed, which consists of hydrophilic domains interdispersed with the cross-linked units. The driving force for formation of the hydrophilic domains is the attractive force among polar molecules in these domains, including unreacted, low molecular mass, partially polymerized molecules and chromophores. This model satisfactorily explains why the inhomogeneous degradation occurs during exposure to UV. Information on the degradation mode and the nature of the nanoscale regions where the major degradation reactions occur should help to design more environmentally stable coatings. Finally, although knowledge of the chemical composition of the hydrophilic domains is not complete at this time, the information on the degradation mode provided by this study should help to develop better conceptual and mathematical models for predicting the service life of crosslinked polymeric coatings exposed to aggressive UV environments.

References

- Kamal, M, Huang, B, "Natural and Artificial Weathering of Polymers." In: Hamid, S, Amin, M, Maadhah, A (eds.) *Handbook of Polymer Degradation*, pp. 127–178. Marcel Dekker, New York, 1992
- Ranby, B, Rabek, JF, *Photodegradation, Photooxidation, and Photostabilization of Polymers, Principles and Applications*, pp. 42–50. Wiley and Sons, New York, 1975
- Rabek, JF, *Polymer Photodegradation—Mechanisms and Experimental Methods*, p. 4. Chapman & Hall, New York, 1995
- Magonov, SN, Heaton, MG, "Atomic Force Microscopy, Part 6: Recent Development in AFM of Polymers." *Am. Lab.*, **30** 9–15 (1998)
- Magonov, SN, Whangbo, M-H, *Surface Analysis with STM/AFM*. Wiley & Sons, New York, 2007
- Knoll, A, Magerle, R, Krausch, G, "Tapping Mode Atomic Force Microscopy on Polymers: Where Is the True Sample Surface?" *Macromolecules*, **34** 4159 (2001)
- Gu, X, Stanley, D, Byrd, E, Dickens, B, Meeker, W, Nguyen, T, Martin, JW, "Linking Accelerated Laboratory Test with Outdoor Performance Results for a Model Epoxy Coating System." In: Martin, JW, Ryntz, RA, Chin, JW, Dickie, RA (eds.) *Service Life Prediction of Polymeric Materials*, pp. 1–43. Springer, New York, 2009
- Martin, JW, Nguyen, T, Byrd, WE, Dickens, B, Embree, N, "Relating Laboratory and Outdoor Exposures of Acrylic Melamine Coatings: I. Cumulative Damage Model and Laboratory Experiment Apparatus." *Polym. Degrad. Stab.*, **75** 193 (2002)
- VanLandingham, MR, Nguyen, T, Byrd, WE, Martin, JW, "On the Use of the Atomic Force Microscope to Monitor Physical Degradation of Polymeric Coating Surfaces." *J. Coat. Technol.*, **73** (923) 43 (2001)
- Nguyen, T, Martin, JW, Byrd, WE, Embree, N, "Relating Laboratory and Outdoor Exposures of Coatings: II. Effects of Relative Humidity on Photodegradation of Acrylic Melamine." *J. Coat. Technol.*, **74** (932) 31 (2002)
- Gu, X, Raghavan, D, Ho, DL, Sung, L, VanLandingham, MR, Nguyen, T, "Nanocharacterization of Surface and Interface of Different Epoxy Networks." *Mater. Res. Soc. Symp.*, **710**, DD10.9 (2002)
- Gu, X, Martin, D, Martin, WJ, Nguyen, T, "Surface, Interface, and Bulk Microstructure of Amine-cured Epoxies—An Intensive AFM Study." In: Chaudhury, M (ed.) *Proc., Adhesion Society Meeting*, p. 507, 2004
- Gu, X, Nguyen, T, Sung, L, VanLandingham, M, Fasolka, M, Martin, WJ, Jean, YC, Nguyen, D, Chang, NK, Wu, T-Y, "Advanced Techniques for Nanocharacterization of Polymeric Coatings." *J. Coat. Technol. Res.*, **1** (3) 191 (2004)
- Chen, X, McGurk, SL, Davies, MC, Roberts, CJ, Shakesheff, KM, Tendler, SJB, Williams, PM, "Chemical and Morphological Analysis of Surface Enrichment in a Biodegradable Polymer Blend by Phase-Detection Imaging Atomic Force Microscopy." *Macromolecules*, **31** 2278 (1998)
- Pienka, Z, Oike, H, Tezuka, Y, "Atomic Force Microscopy Study of Environmental Responses on Poly(vinyl alcohol)-graft-Polystyrene Surfaces." *Langmuir*, **15** 3197 (1999)
- VanLandingham, MR, Eduljee, RF, Gillespie, JW, "Relationship Between Stoichiometry, Microstructure, and Properties of Amine-Cured Epoxies." *J. Appl. Polym. Sci.*, **71** 699 (1999)
- Gu, X, Raghavan, D, Nguyen, T, VanLandingham, M, "Characterization of Polyester Degradation in Alkaline Solution using Tapping Mode Atomic Force Microscopy: Exposure to Alkaline Solution at Room Temperature." *Polym. Degrad. Stab.*, **74** 139 (2001)
- Bar, G, Thomann, Y, Brandsch, R, Whamgho, MH, "Factors Affecting the Height and Phase Images in Tapping Mode Atomic Force Microscopy. Study of Phase-separated Polymer Blends of Poly(ethene-co-styrene) and Poly(2,6-dimethyl-1,4-phenylene oxide)." *Langmuir*, **13** 3807 (1997)
- Magonov, SN, Elings, V, Whangbo, MH, "Phase Imaging and Stiffness in Tapping Mode Atomic Force Microscopy." *Surf. Sci.*, **375** L385 (1997)
- Cuthrell, RE, "Epoxy Polymers. II. Macrostructure." *J. Appl. Polym. Sci.*, **12** 1263 (1968)
- Giraud, M, Nguyen, T, Gu, X, VanLandingham, MR, "Effects of Stoichiometry and Epoxy Molecular Mass on Wettability and Interfacial Microstructures of Amine-Cured Epoxies." In: Emerson, JA (ed.) *Proc. Adhesion Society Meeting*, p. 260, 2001
- Rezig, A, Nguyen, T, Martin, D, Sung, L, Gu, X, Jasmin, J, Martin, JW, "Relationship Between Chemical Degradation and Thickness Loss of an Amine-cured Epoxy Coating Exposed to Different UV Environments." *J. Coat. Technol. Res.*, **3** (3) 173 (2006)
- Bellinger, V, Bouchard, C, Claveirolle, P, Verdu, J, "Photooxidation of Epoxy Resins Cured by non-Aromatic Amines." *Photochemistry*, **1** 69 (1981)
- Bellinger, V, Verdu, J, "Oxidative Skeleton Breaking in Epoxy-Amine Networks." *J. Appl. Polym. Sci.*, **30** 363 (1985)
- Lemaire, J, Siampiringue, N, "Prediction of Coating Lifetime Based on FTIR Microspectrophotometric Analysis of Chemical Evolutions." In: Bauer, D, Martin, JW (ed.) *Service Life Prediction of Organic Coatings—A System*

- Approach*, American Chemical Society Series 722, pp. 246–256. Oxford Press, New York, 1999
26. Nguyen, T, Martin, JW, Byrd, WE, Embree, N, “Relating Laboratory and Outdoor Exposures of Coatings: IV Mode and Mechanism of Hydrolysis of Acrylic-Melamine Coatings.” *J. Coat. Technol.*, **75** (941) 37 (2003)
 27. Nguyen, T, Martin, JW, Byrd, WE, Embree, N, “Relating Laboratory and Outdoor Exposure of Coatings: III. Effects of Relative Humidity on Moisture-Enhanced Photolysis of Acrylic-Melamine Coatings.” *Polym. Degrad. Stab.*, **77** 1 (2002)
 28. Bauer, D, Gerlock, JL, Mielewski, D, “Photostabilization and Photodegradation in Organic Coatings Containing a Hindered Amine Light Stabilizer, Part VII. Halt Effectiveness in Acrylic-Melamine Coatings Having Different Free Radical Formation Rates.” *Polym. Degrad. Stab.*, **36** 9 (1992)
 29. Karyakina, MI, Kuzmak, AE, “Protection by Organic Coatings: Criteria, Testing Methods and Modelling.” *Prog. Org. Coat.*, **18** 325 (1990)
 30. Bascom, WD, “Water at the Interface.” *J. Adhesion*, **2** 168 (1970)
 31. Mills, DJ, Mayne, JEO, “The Inhomogeneous Nature of Polymer Films and Its Effects on Resistance Inhibition.” In: Leiheiser, H, Jr, (ed.) *Corrosion Control by Organic Coatings*, pp. 12–17. Nat. Assoc. Corr. Eng., Houston, TX, 1981
 32. Fernandez, PR, Corti, H, “Epoxy Coal Tar Films: Membrane Properties and Film Deterioration.” *J. Coat. Technol.*, **49** (632) 62 (1977)
 33. Corti, H, Fernandez, PR, Gomez, D, “Protective Organic Coatings: Membrane Properties and Performance.” *Prog. Org. Coat.*, **10** 5 (1982)
 34. Gu, X, Sung, L, Kidah, B, et al., “Multiscale Physical Characterization of an Outdoor-Exposed Polymeric System.” *J. Coat. Technol. Res.*, **6** (1) 67 (2009)
 35. Pospíšil, J, Pilař, J, Billingham, NC, Marek, A, Horák, Z, Nešpůrek, S, “Factors Affecting Accelerated Testing of Polymer Photostability.” *Polym. Degrad. Stab.*, **91** 417 (2005)
 36. George, GA, Celina, M, “Homogeneous and Heterogeneous Oxidation of Polypropylene.” In: Hamid, SH (ed.) *Handbook of Polymer Degradation*, pp. 277–311. Marcel Dekker, Inc., New York, 2000
 37. Richard, J, Mignaud, C, Wong, K, “Water Vapour Permeability, Diffusion and Solubility in Latex Films.” *Polym. Int.*, **30** 431 (1993)
 38. Fischer, M, Tran, CD, “Evidence for Kinetic Inhomogeneity in the Curing of Epoxy Using the Near-Infrared Multispectral Imaging Technique.” *Anal. Chem.*, **71** 953 (1999)
 39. Mayne, JEO, Scantlebury, JD, “Ionic Conduction in Polymer Films, Part II, Br.” *Polymer*, **2** 240 (1970)
 40. Mayne, JEO, Mills, DJ, “The Effect of the Substrate on the Electrical Resistance of Polymer Films.” *J. Oil Color Chem. Assoc.*, **58** 155 (1975)
 41. Wu, CL, Zhou, XJ, Tan, YJ, “A Study on the Electrochemical Inhomogeneity of Organic Coatings.” *Prog. Org. Coat.*, **25** 379 (1995)
 42. Walker, P, “Effect of Water on the Adhesion of Surface Coatings.” *Off. Digest*, **12** (491) 1561 (1965)
 43. Kelleher, PG, Gesner, BD, “Photo-oxidation of Phenoxy Resin.” *J. Appl. Polym. Sci.*, **13** 9 (1969)
 44. Göpferich, A, “Polymer Bulk Erosion.” *Macromolecules*, **30** 2598 (1997)
 45. Berge, A, Kvaeven, B, Ugelstad, J, “Melamine-Formaldehyde Compounds II: Acid Decomposition of Methylol Melamines and Methoxymethyl Melamines.” *Eur. Polym. J.*, **6** 981 (1970)
 46. Bauer, DR, “Degradation of Organic Polymers. I. Hydrolysis of Melamine Formaldehyde/Acrylic Copolymer Films.” *J. Appl. Polym. Sci.*, **27** 3651 (1982)
 47. Ioselevich, AS, Kornyshev, AA, Steinke, JHG, “Fine Morphology of Proton-Conducting Ionomers.” *J. Phys. Chem.*, **108** 11953 (2004)
 48. Israelachvili, JN, *Intermolecular and Surface Forces*, 2nd ed., pp. 139–149. Academic Press, New York, 1992